2.E Angular Distributions of High-Order Harmonics from Low-Density Gas Targets

High-order harmonics have been observed during laser-atom interactions at a number of different laser wavelengths with short-pulse, high-intensity laser systems. Harmonics with frequencies in excess of 100 times the laser frequency have been reported.[1–3]

Most high-order, harmonic-generation experiments to date have used gas target pressures in excess of 10 Torr. These high pressures have been used to enhance the harmonic signal, which increases quadratically with the pressure. The phase-mismatch factors (caused by both neutral and ionized media) increase with the pressure as does the effect of refraction of the incident laser when the medium becomes ionized. Very few measurements of the angular distributions of the high-order harmonics have been reported.[3] The far-field pattern can provide additional insight into the laser propagation, phase matching, and the atomic response.

Phase-matching effects have been extensively studied by L'Huillier and co-workers.[1,4–7] They have made many detailed comparisons of their calculations with their experiments and have found excellent agreement. Their studies have included the effect of the intensity, pressure, and focusing characteristics (both confocal parameter and jet position relative to the focus) on the spatially and temporally integrated harmonic output. Faldon *et al.*[8] have been able to explain the temporal history of the harmonic emission by considering the effects of ionization and phase matching.

In this article, observations of the angular (far-field) distribution of high-order harmonic generation with a low-density gas target with gas pressures of the order of 0.5 Torr are presented. With the *f*/70 focal system and 1-mm-thick target, the phase-mismatch factors from neutral gas, free electrons, and geometric effects are all less than π. Thus, in these experiments, the high-order harmonics are generated under conditions where the effects of phase mismatch on the harmonic generation should be minimized. The goal of this work is to separate the atomic response from the effects of phase matching. In the experiments presented in this article, the far-field distribution of the 11th to 21st harmonics of the incident laser radiation has been observed. The article is organized as follows: The laser system and the detector are described first, followed by the onset of refraction, which constrains the experimental conditions. Next, the angular distributions of the high-order harmonics are presented, followed by a comparison of the measurements with the predictions of lowest-order perturbation theory. Finally, the conclusions are presented. (The gas target is described in Sec. 2.F.)

Experimental Conditions

The high-order harmonics are observed by focusing a 1-μm, 1.5-ps laser into a moderate-density gas target (p ~0.5 Torr, thickness ~1 mm) and then detecting the harmonics with a transmission grating coupled to an MCP-phosphor image intensifier. A schematic of the experiment is shown in Fig. 54.18. The various

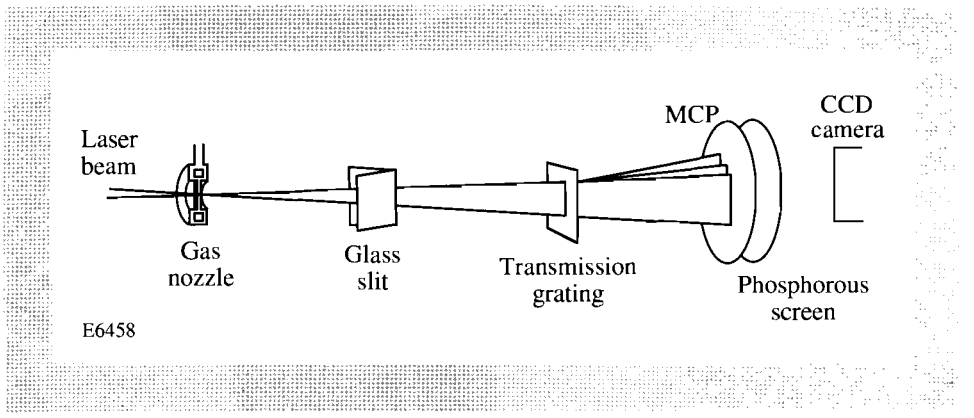

Fig. 54.18
Schematic of the experimental setup, including the gas target and the angularly resolved spectrometer.

components of the experimental setup are discussed in this section, as is the effect of refraction on the operating conditions.

The 1-μm, 1.5-ps laser pulses used to generate the harmonics are generated with an Nd:glass, chirped-pulse-amplification laser system,[9,10] which has been described in detail elsewhere.[11] We have recently upgraded the energy capability and focusing quality of the system.

For these experiments, a long Rayleigh range is desired to minimize the geometric phase-matching effects on the high-order harmonics. To increase the *f*-number of the focusing system, a smaller-than-usual, 1.1-cm-radius beam is produced by the laser system. Under these conditions, the laser energy is limited to less than 300 mJ to avoid *B*-integral effects and to operate significantly below the compression-grating damage threshold. This beam is focused with a 153-cm lens to produce an *f*-number of 70. While the use of the long-focal-length lens sacrifices peak field intensity, the system is still able to achieve 3×10^{15} W/cm^2 with relatively large focal volumes and low field gradients. The experiments are currently limited to much lower energies because of plasma formation in the spectrometer.

The focal spot diameter is 1.2 times diffraction limited. The focal characteristics of the laser were measured by direct imaging, with 4X magnification, onto a CCD camera. The focal-spot radius as a function of the axial distance along the focus is shown in Fig. 54.19, as is the calculated radius for a diffraction-limited *f*/70 beam.

The spectrometer used in these experiments consists of a slit with approximate dimensions of 500 μm × 2.5 cm followed by a bare gold wire transmission grating, consisting of 0.5-μm-diam gold wires, separated by 1 μm (center to center). The slit is aligned parallel to the grating wires. Following the grating is a microchannel-plate (MCP), image-intensified phosphor screen (Galileo model 8081). The microchannel-plate intensifier is not UV enhanced so it cannot detect harmonics lower than the ninth. The light incident on the slit and grating is dispersed by the grating and produces spectral lines on the phosphor screen. The different harmonic orders are separated in the direction perpendicular to the grating lines, and their angular distributions are observed parallel to the slit. Thus information about the far-field pattern as well as the spectral content of the harmonics is obtained simultaneously. At this time, the spectrometer is not

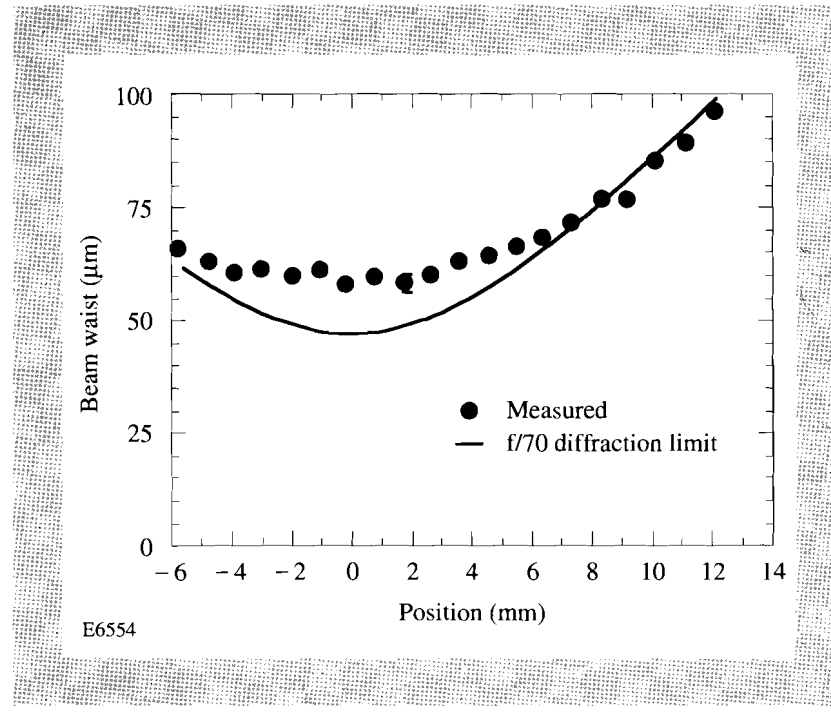

Fig. 54.19
Plot of the measured laser-beam waist as a function of axial position along the focus, showing that the beam is 1.2 times diffraction limited with *f*/70 optics.

absolutely calibrated so only relative levels of harmonic emission are presented. In all cases, the same relative units are used. The relatively large slit allows a larger photon flux to reach the detector at the cost of reduced spectral resolution. In the configuration used for the experiments presented in this article, the harmonic lines begin to overlap with the 23rd harmonic.

The gas target is designed to create well-characterized, narrow gas distributions at low densities (1–2 Torr or less with backing pressures up to 5–10 Torr).[12] This low-density regime is desirable to reduce the phase-matching effects during the harmonic generation[5] and the effects of refraction of the focused laser beam. Also, the low backing pressure has the advantage of reducing the possibility of dimer formation in gases such as Xe.[13]

The target and its calibration are described in more detail in the next article in this volume. The gas target is 1 mm thick and typically operated at pressures of 1 Torr or less. One important goal of the experiments is to operate in a regime where the laser propagation through the target is unaffected by the medium. This makes the interpretation of the experimental results easier. A laser propagating through an ionized medium may undergo refraction or self-focusing. The laser was focused through the gas target and imaged onto a CCD camera with various xenon gas pressures in the target and with various peak laser intensities. The results are shown in Fig. 54.20. Figures 54.20(a)–54.20(c) show the change in effective focal spot with increasing laser intensity at 0.6-Torr pressure. At the highest intensity xenon is fully ionized within the focal volume.[14] At this low pressure, the focal spot is identical to that observed in the vacuum. When the pressure is increased to 2 Torr as in Figs. 54.20(d)–54.20(f), an apparent decrease in the focal volume is observed. This is caused by refraction, which decreases the *f*-number of the laser as it leaves the gas target. Preliminary calculations of the refraction under these conditions are consistent with the observed results.

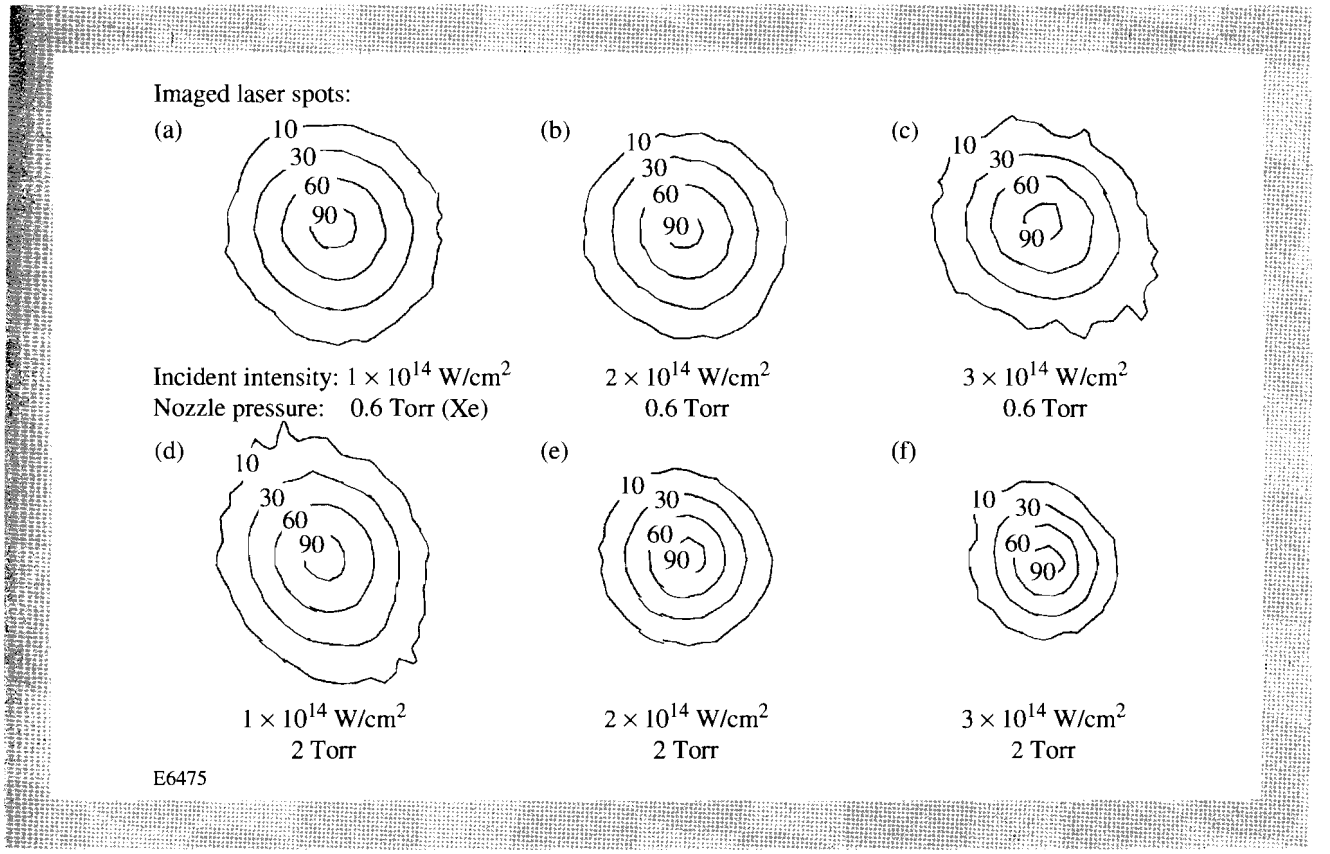

Fig. 54.20
Images of the laser focus as a function of laser intensity and gas target pressure. Figures 54.20(a)–54.20(c) show increasing laser intensity at 0.6 Torr of xenon pressure, and Figs. 54.20(d)–54.20(f) show the same for 2 Torr of xenon.

Harmonic Far-Field Distributions

The experimental conditions previously described have been chosen to minimize the phase-mismatch factors.[5] The combination of *f*/70 focusing and a thin gas target (1 mm) means that the target thickness is much less than the 12-mm confocal parameter. In addition, the low gas pressures of ~0.5 Torr mean that the phase mismatch from neutral Xe and free electrons is minimal. Table 54.I shows that the phase-mismatch factors for various harmonic orders are less than or of the order of 1 rad.

Table 54.I: Phase-mismatch factors ΔkL (radians).

Harmonic order	9	13	17	21
Neutral Xe	0.08	−0.05	−0.08	−0.08
Free electrons	0.50	0.70	0.90	1.10

E6543

Figure 54.21 shows the far-field (angular) distribution of the 11th to 21st harmonics of the laser at an intensity of 9×10^{13} W/cm^2 and a gas target peak pressure of 0.3 Torr xenon. These results are typical of the harmonic profiles under these conditions. Most of the high-order harmonics have a very narrow angular structure. For xenon under these conditions, large-scale shoulder structures appear on the 13th harmonic. The shoulders are also observed on the 15th harmonic in krypton and the 17th in argon. While the strongest shoulders are observed on the 13th harmonic in xenon, recent, more sensitive experiments have shown shoulders on other harmonics as well.

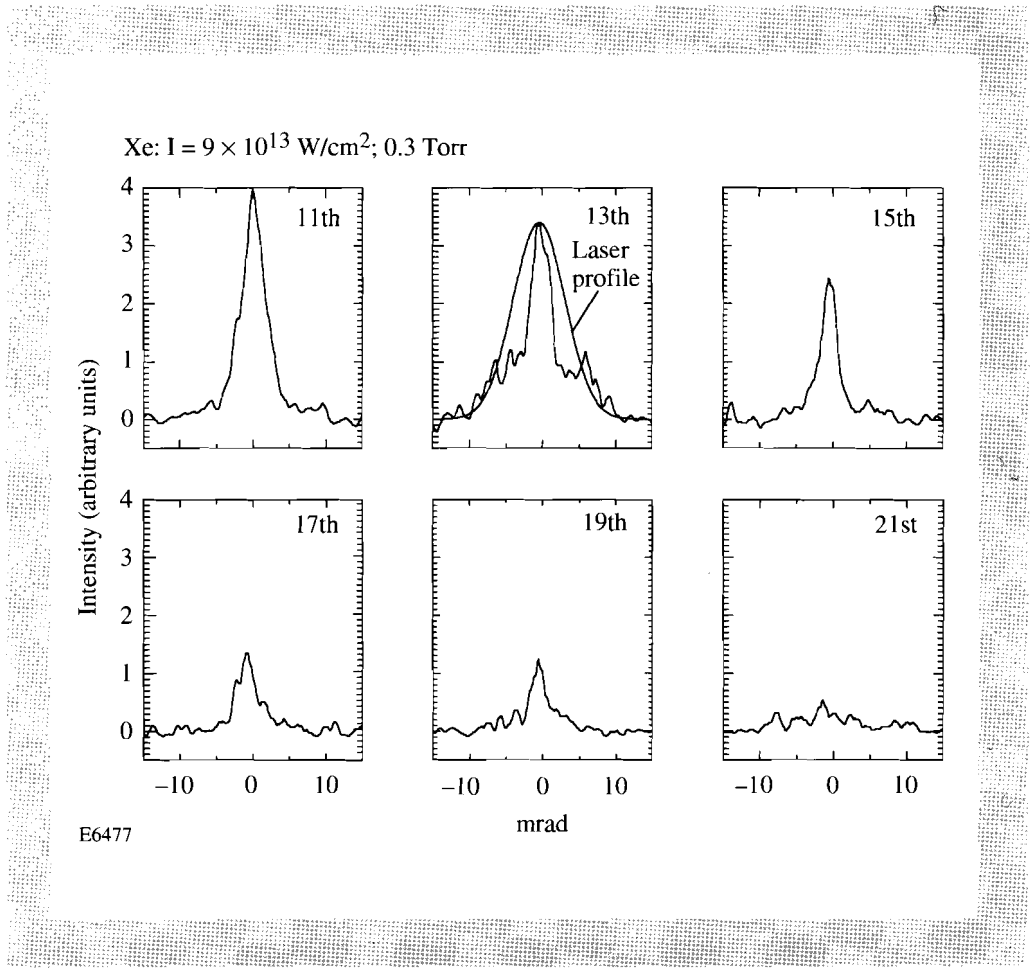

Fig. 54.21
Typical far-field distribution of the 11th to 21st harmonic observed for 0.3 Torr of xenon at 9×10^{13} W/cm^2.

The relative energy in the different harmonics is determined by integrating the harmonic emission radially, taking the circularly symmetric nature of the emission into account:

$$E_q = \int_0^\infty 2\pi I(r)\, r dr \, .$$

The emission is symmetric around the peak signal level. Figure 54.22 shows the relative energy in the 11th to 23d harmonics in xenon at a gas pressure of 0.5 Torr for three different intensities. The development of a plateau in the harmonic emission with increasing intensity is evident.

Under perfect phase-matching conditions, the integrated harmonic intensity should scale as N^2, where N is the number of atoms in the focal volume for a fixed intensity. Figure 54.23 shows the integrated energy for the 11th to 21st harmonic in xenon at 9×10^{13} W/cm^2 at four different gas pressures. The overall shape of the harmonic-energy spectrum is maintained, and the energy of each harmonic scales quadratically with pressure as expected.

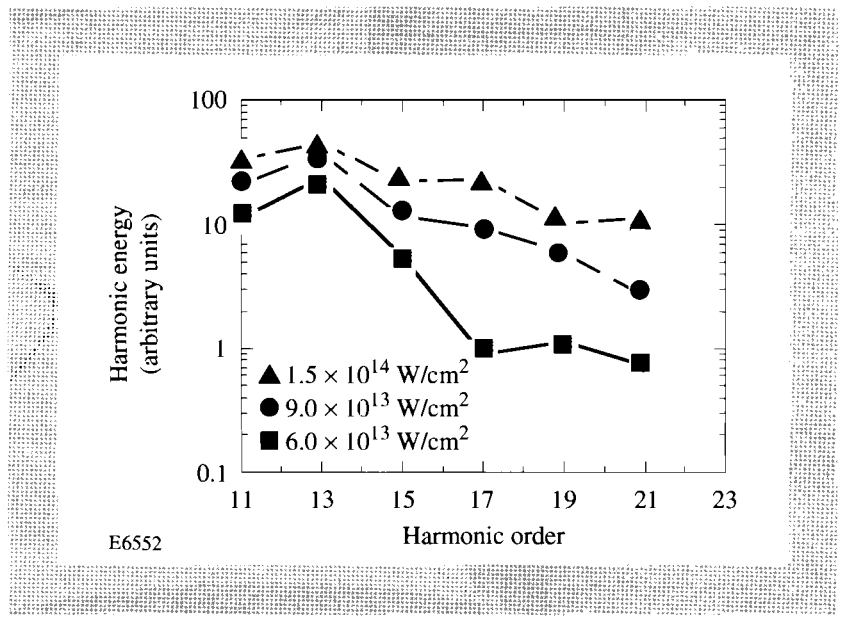

Fig. 54.22
Relative-harmonic energy in the 11th to 21st harmonic in xenon at 0.5 Torr and three different intensities.

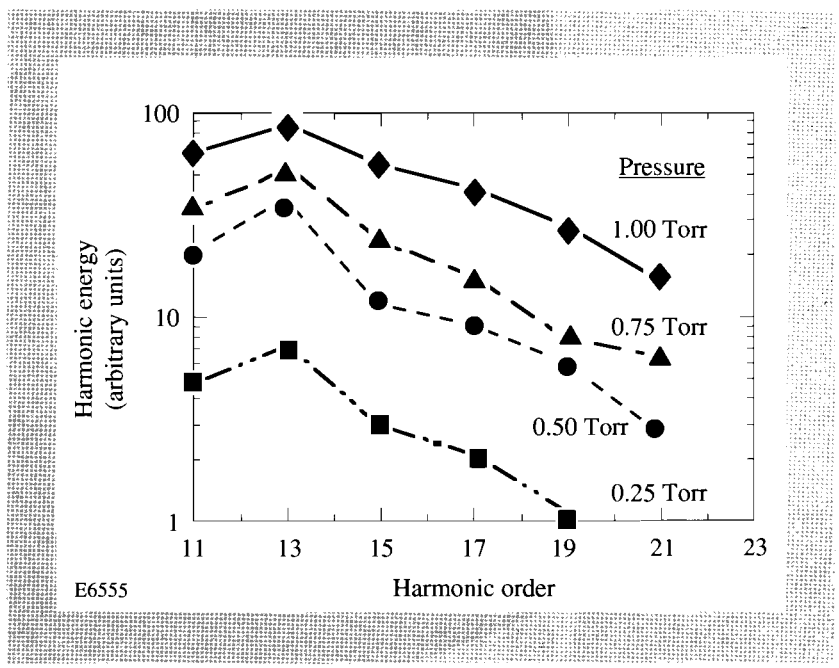

Fig. 54.23
Integrated energy for the 11th through 21st harmonic for xenon at 9×10^{13} W/cm^2 for four different gas pressures.

One of the features common to all of the low-pressure, far-field distributions is the development of significant shoulders, which appear most pronounced on one particular harmonic first. This is evident in the 13th harmonic in xenon in Fig. 54.21. The far-field emission for Xe, Kr, and Ar is shown in Fig. 54.24. For Kr and Ar, the shoulders appear on the 15th and 17th harmonics, respectively. In this case, the intensity is approximately the barrier suppression ionization threshold (BSI),[15] and the gas target density has been scaled so that the level of emission is similar in each case. At the BSI threshold, the ionization probability has been observed to be approximately 1% for 1.5-ps, 1-μm laser pulses.[14,15] It is important to note the similarities among the far-field patterns of the different harmonics. Each of the harmonics shows the same shapes. In fact, the angular distributions are almost identical. The primary difference is the harmonic on which the shoulders first appear. These results are summarized in Table 54.II. The pronounced structure appears on the harmonic, which is one order ($2\omega_L$) higher than the first with energy greater than the field-free atomic ionization potential.

Comparisons with Lowest-Order Perturbation Theory

With the exception of the harmonic, which shows the shoulder-like structure, the far-field patterns are quite narrow and seem to get narrower with increasing harmonic order. We can compare the far-field widths with the predictions of

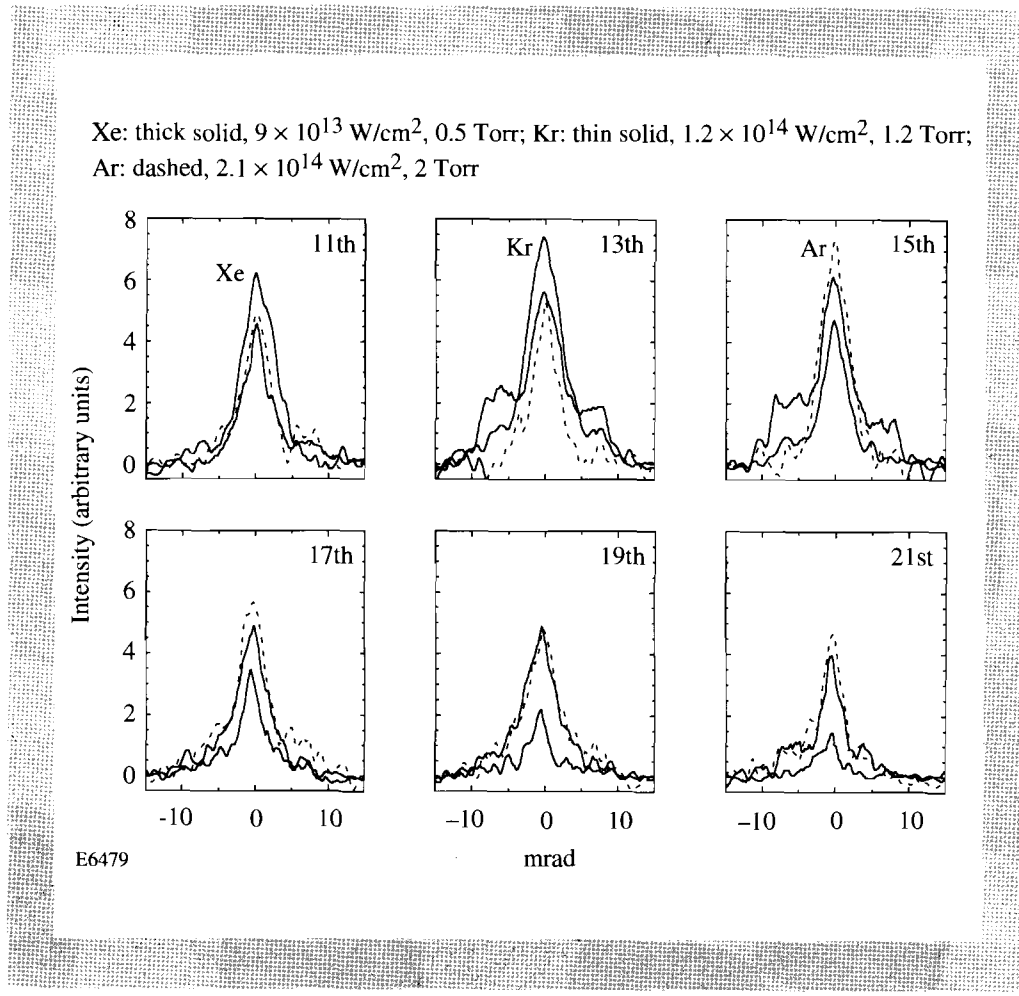

Fig. 54.24
Comparison of the far-field emission for Xe, Kr, and Ar with the intensity at the BSI threshold.

Table 54.II: Comparison of harmonic structure in different target gases.

Target Gas	BSI Intensity[15]	Experimental Intensity	First Harmonic Showing Structure
Xenon	8.6×10^{13} W/cm^2	9×10^{13} W/cm^2	13
Krypton	1.5×10^{14} W/cm^2	1.2×10^{14} W/cm^2	15
Argon	2.5×10^{14} W/cm^2	2.1×10^{14} W/cm^2	17

E6544

lowest-order perturbation theory (LOPT). The harmonic intensity is assumed to vary as I^q. The angular width of the harmonics is then expected to vary as $\delta\theta_o / \sqrt{q}$, where $\delta\theta_o$ is the angular distribution of the laser. The observed harmonic emission for Kr at 0.5 Torr and 10^{14} W/cm^2 is compared with the LOPT predictions in Fig. 54.25. Good agreement with the far-field patterns of all the harmonics is observed. It should be noted though, that the relative intensity of each harmonic does not scale with intensity as LOPT would predict.

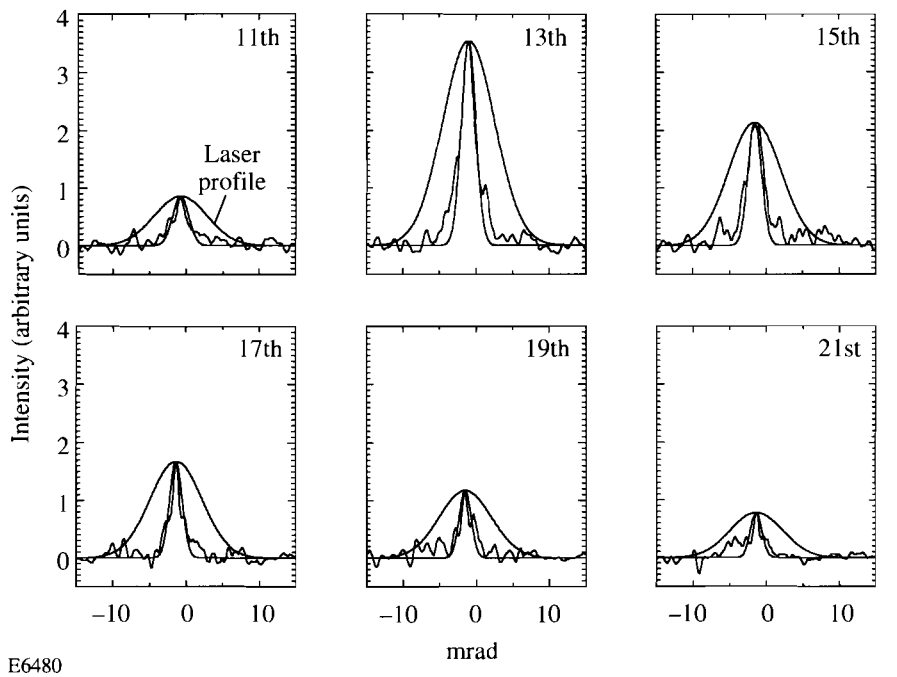

Fig. 54.25
Comparison of the far-field emission for Kr at 0.5 Torr and 1×10^{14} W/cm^2 with the predictions of lowest-order perturbation theory.

Conclusion

The far-field pattern of high-order harmonics has been observed under conditions where the geometric and propagation phase-mismatch factors should be negligible. Under these conditions, we find that the far-field pattern (though not the intensity scaling) is consistent with lowest-order perturbation theory, except for one harmonic (the 13th in xenon, the 15th in Kr, and the 17th in Ar). The harmonic emission scales quadratically with the pressure and, even under these low-pressure conditions, a plateau develops, as has been observed in many other experiments.

ACKNOWLEDGMENT

This work is supported by the National Science Foundation under contract PHY-9200542. Additional support was provided by the U.S. Department of Energy Office of Inertial Confinement Fusion under Cooperative Agreement No. DE-FC03-92SF19460 and the University of Rochester. The support of DOE does not constitute an endorsement by DOE of the views expressed in this article.

REFERENCES

1. A. L'Huillier and Ph. Balcou, Phys. Rev. Lett. **70**, 774 (1993).
2. J. J. Macklin, J. D. Kmetec, and C. L. Gordon III, Phys. Rev. Lett. **70**, 766 (1993).
3. R. A. Smith *et al.*, "Recent Ultra-High Harmonic Generation Experiments with Picosecond Laser Pulses," to be published in the *Proceedings of the NATO Workshop on Super-Intense, Laser-Atom Physics*, edited by B. Piraux, Han-sur-Lesse, Belgium, 8–14 January 1993.
4. A. L'Huillier, K. J. Schafer, and K. C. Kulander, Phys. Rev. Lett. **66**, 2200 (1991).
5. A. L'Huillier, K. J. Schafer, and K. C. Kulander, J. Phys. B: At. Mol. Opt. Phys. **24**, 3315 (1991).
6. A. L'Huillier, P. Balcou, and L. A. Lompré, Phys. Rev. Lett. **68**, 166 (1992).
7. A. L'Huillier *et al.*, Phys. Rev. A **46**, 2778 (1992).
8. M. E. Faldon *et al.*, J. Opt. Soc. Am. B **9**, 2094 (1992).
9. D. Strickland and G. Mourou, Opt. Commun. **56**, 219 (1985).
10. P. Maine, D. Strickland, P. Bado, M. Pessot, and G. Mourou, IEEE J. Quantum Electron. **24**, 398 (1988).
11. Y.-H. Chuang, D. D. Meyerhofer, S. Augst, H. Chen, J. Peatross, and S. Uchida, J. Opt. Soc. Am. B **8**, 1226 (1991).
12. J. Peatross and D. D. Meyerhofer, submitted to *Review of Scientific Instruments*.
13. L. A. Lompré *et al.*, J. Appl. Phys. **63**, 1791 (1988).
14. S. Augst, D. D. Meyerhofer, D. Strickland, and S. L. Chin, J. Opt. Soc. Am. B **8**, 858 (1991).
15. S. Augst, D. Strickland, D. D. Meyerhofer, S. L. Chin, and J. H. Eberly, Phys. Rev. Lett. **63**, 2212 (1989).